JACS
JOURNAL OF THE AMERICAN CHEMICAL SOCIETY
Article
pubs.acs.org/JACS

β-Technetium Dichloride: Solid-State Modulated Structure, Electronic Structure, and Physical Properties

Christos D. Malliakas,[#,¶] Frederic Poineau,[†] Erik V. Johnstone,[†] Philippe F. Weck,[‖] Eunja Kim,[§] Brian L. Scott,[‡] Paul M. Forster,[†] Mercouri G. Kanatzidis,[#,¶] Kenneth R. Czerwinski,[†] and Alfred P. Sattelberger*[,#,⊥,†]

[#]Department of Chemistry, Northwestern University, Evanston, Illinois 60208, United States
[†]Department of Chemistry, University of Nevada Las Vegas, Las Vegas, Nevada 89154, United States
[‖]Sandia National Laboratories, Albuquerque, New Mexico 87185, United States
[§]Department of Physics and Astronomy, University of Nevada Las Vegas, Las Vegas, Nevada 89154, United States
[‡]Materials Physics and Applications Division, Los Alamos National Laboratory, Los Alamos, New Mexico 87545, United States
[¶]Materials Science Division, Argonne National Laboratory, Argonne, Illinois 60439, United States
[⊥]Energy Engineering and Systems Analysis Directorate, Argonne National Laboratory, Argonne, Illinois 60439, United States

Supporting Information

ABSTRACT: A second polymorph of technetium dichloride, β-$TcCl_2$, has been synthesized from the reaction of Tc metal and chlorine in a sealed tube at 450 °C. The crystallographic structure and physical properties of β-$TcCl_2$ have been investigated. The structure of β-$TcCl_2$ consists of infinite chains of face sharing [Tc_2Cl_8] units; within a chain, the Tc≡Tc vectors of two adjacent [Tc_2Cl_8] units are ordered in the long-range where perpendicular and/or parallel arrangement of Tc≡Tc vectors yields a modulated structure. Resistivity and Seebeck measurements performed on a β-$TcCl_2$ single crystal indicate the compound to be a p-type semiconductor while a magnetic susceptibility measurement shows technetium dichloride to be diamagnetic. A band gap of 0.12(2) eV was determined by reflectance spectroscopy measurements. Theoretical calculations at the density functional level were utilized for the investigation of other possible stable forms of $TcCl_2$.

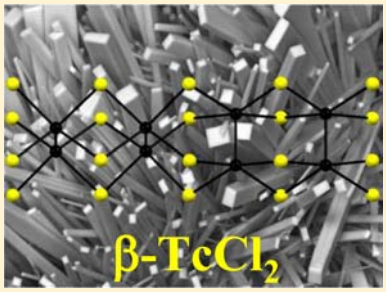

INTRODUCTION

Transition metal dichlorides exhibit catalytic, photochemical and redox properties that are of interest for industrial and medical applications.[1−6] Since the discovery of molybdenum dichloride in 1859,[7] second and third row transition metal dichlorides have also been reported for six other elements (Zr,[8] Hf,[9] W,[10] Tc,[11] Pd,[12] and Pt[13]). Currently, 11 dichloride phases are structurally characterized, the last dichloride to be reported being $TcCl_2$ in 2011.[11] Technetium dichloride was initially obtained from the reaction of Tc metal and chlorine in a sealed tube at 450 °C.[11] After the reaction, a dark crystalline powder that contains $TcCl_2$ was obtained at the hot end of the tube, and some needles (β-$TcCl_2$) were observed on the center part of the tube. The black powder was treated with aluminum trichloride ($AlCl_3$) at 450 °C in a sealed tube and $TcCl_2$ crystals (α-$TcCl_2$) were obtained at the end of the tube. The structure of α-$TcCl_2$ consists of infinite chains of triply metal−metal bonded Tc_2Cl_8 units (Chart 1).[11] Theoretical calculations confirmed the presence of Tc≡Tc triple bonds and predicted α-$TcCl_2$ to be a semiconductor and diamagnetic, but no physical measurements were reported. The structure of the β-$TcCl_2$ crystals has been investigated recently by Extended X-ray Absorption Fine Structure spectroscopy (EXAFS); the results were consistent with the presence of face sharing Tc_2Cl_8 units within the compound.[14] Interestingly, the structure of β-$TcCl_2$ consists of two orientations of Tc≡Tc vectors where the Tc≡Tc vectors of two adjacent Tc_2Cl_8 units are either parallel or perpendicular (Chart 1). In the present work, we characterized the structure of β-$TcCl_2$ using a multidimensional crystallographic approach and measured its magnetic susceptibility, resistivity, and band gap. Additionally, the structure and properties of α/β-$TcCl_2$ are analyzed by theoretical methods.

EXPERIMENTAL SECTION

Caution. Technetium-99 is a weak beta emitter (E_{max} = 292 keV). All manipulations were performed in a radiochemistry laboratory designed for chemical synthesis using efficient HEPA-filtered fume hoods, Schlenk and glovebox techniques, and following locally approved radioisotope handling and monitoring procedures. The starting compound NH_4TcO_4 was purchased from Oak Ridge National Laboratory. Tc metal was prepared according to the method previously reported.[11] Lecture bottles of Cl_2 gas were purchased from Sigma-Aldrich and used without further purification.

Received: August 15, 2013
Published: September 20, 2013

   dx.doi.org/10.1021/ja408459k | J. Am. Chem. Soc. 2013, 135, 15955−15962

Chart 1. View of a α-$TcCl_2$ Chain along the *c*-Axis of the Unit Cell (Top); View of the Local Structure of β-$TcCl_2$ Suggested by EXAFS Spectroscopy (Bottom)[a]

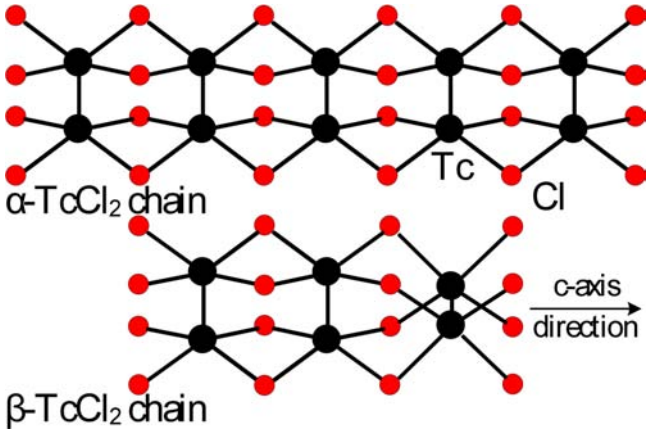

[a]Tc and Cl atoms are in black and red, respectively.

Preparation of β-$TcCl_2$. The compound was prepared by reacting Tc metal and Cl_2 (Tc:Cl, 1:2.5) at 450 °C in a Pyrex sealed tube for 24 h according the method previously reported (Supporting Information S1).[11] After the reaction, the β-$TcCl_2$ crystals obtained at the center of the tube were used for the structure determination and conductivity measurements without any further thermal treatment. The powder obtained at the hot end of the tube was used for magnetic and band gap measurements. X-ray powder diffraction measurements (Figure S1) show the powder to contain Tc metal and $TcCl_2$.

Single Crystal X-ray Diffraction (SCXRD). Intensity data were collected on a STOE IPDS 2T diffractometer equipped with a graphite monochromatized Mo radiation (λ = 0.71073 Å) source and an Image Plate (IP) detector. The data were collected with an ω-scan technique from 0 to 180° and an arbitrary φ-angle. Data reduction was performed with the X-Area package.[15] The length determination and refinement of the *q*-vectors was performed with the Peaklist 2.01 software part of the X-Area suite using a least-squares refinement algorithm. An analytical absorption correction was performed (X-Shape within X-Area) and all structures were refined with JANA2006 software.[16] Direct methods of SHELXTL software[17] were used to find the atomic positions in the subcell. The distortion (positional or temperature parameter) of a given atomic parameter x_4 in the subcell can be expressed by a periodic modulation function $p(x_4)$ in a form of a Fourier expansion (eq 1):

$$p(k + x_4) = \sum_{n=1}^{m} A_{sn} \sin[2\pi \overline{q}_n (k + x_4)] + \sum_{n=1}^{m} A_{cn} \cos[2\pi \overline{q}_n (k + x_4)] \quad (1)$$

where A_{sn} is the sinusoidal coefficient of the given Fourier term, A_{cn} is the cosine coefficient, *n* is the number of modulation waves used for the refinement, and *k* is the lattice translation. $\overline{q}_n = \sum_{i=1}^{d} \alpha_{ni} q_i$ where α_{ni} are the integer numbers for the linear combination of the incommensurate modulation vectors q_i. A useful coordinate *t* that characterizes and describes the real three-dimensional structure constructed as a perpendicular intersection with the forth dimensional axis is defined as $t = x_4 - \mathbf{q}\cdot\mathbf{r}$, where **r** is a vector in the real three-dimensional reciprocal space.

Occupational distortions sometimes cannot be described by a relatively small number of harmonic waves as we assumed in the previous case. The occupational modulation pattern may look like a step-like discontinuous function with sharp changes on the occupied fraction from 0 to 1. The so-called Crenel functions are discontinuous periodic functions constructed for the description of such cases. The occupational modulation often occurs as atomic blocks that are occupied by one kind of atom. These blocks can have different width and order. Such a model can be described by a periodic discontinuous modulation function (eq 2):[18]

$$p(x_4) = 1 \text{ for } x_4 \in \langle x_4^0 - \Delta/2, x_4^0 + \Delta/2\rangle$$
$$p(x_4) = 0 \text{ for } x_4 \notin \langle x_4^0 - \Delta/2, x_4^0 + \Delta/2\rangle \quad (2)$$

where Δ and x_4^0 are the width and center of the Crenel function. The Fourier transform of this function gives eq 3,

$$P_m(\Delta, x_4^0) = \exp(2\pi i m x_4^0) \sin(\pi m \Delta)/\pi m \quad (3)$$

that modifies the atomic contribution to the structure factor. Such a modulation induces strong satellites up to very high order. Similarly as for the harmonic modulation, the diffraction pattern has isotropic character but the number of observable satellites is much higher. According to eq 3, intensities of satellites are dropping off as $1/m^2$. The Crenel like modulation was originally introduced to account for a strong occupation modulation in one special structure[19] but nowadays plays a very important role as it allows the description of a general discontinuity in a modulated structure.

The substitutional modulation naturally induces some periodic incommensurate tension in the crystal as the two different atoms cannot generally fit to the same position and coordination. This often causes an additional positional modulation. The Crenel function is applied on the last wave of the overall modulation (possible combination of waves for positional distortion) and it significantly reduces the number of parameters compared to the use of a large number of Fourier series of harmonic waves.

Satellite reflections of first order were observed and used for the refinement of β-$TcCl_2$. A single modulation wave for positional and thermal parameters was used for all Cl atoms. Additionally, an occupational step-like function, Crenel function, was used to describe the discontinuous modulation of the Tc atoms due to the long-range ordering of Tc occupancies. A modulation wave for thermal parameters for Tc was also used. Only the symmetry allowed Fourier terms were refined.

Magnetic Susceptibility. Magnetic susceptibility was measured from 4 K to room temperature using a Quantum Design Magnetic Properties Measurement System (MPMS) superconducting quantum interference device (SQUID) magnetometer. Temperature-dependent magnetic susceptibilities were measured in a gelatin capsule containing 20.1 mg of powdered sample with an applied field of 500 Oe.

Band Gap Measurement. A Nicolet 6700 IR spectrometer equipped with a diffuse-reflectance kit was used for the 4000−400 cm^{-1} spectral region. The spectrum was referenced against a metallic mirror used as a nonabsorbing reflectance standard. The generated reflectance-versus-wavelength data were used to estimate the band gap of the material by converting reflectance to absorbance data according to the Kubelka−Munk equation: $\alpha/S = (1 - R)^2/(2R)$, where *R* is the reflectance and α and *S* are the absorption and scattering coefficients, respectively.[20−22]

Charge Transport Measurements. Four-probe high-temperature electrical resistivity measurements were performed under vacuum from room-temperature to 530 K on the crystal used for the X-ray data collection. Measurements were made for arbitrary current directions in the *ac*-pseudotetragonal plane using standard four point contact geometry. A homemade resistivity apparatus equipped with a nanovoltmeter (Keithley 2182A), precision direct current (DC) source (Keithley 6220), and a high-temperature vacuum chamber controlled by a temperature controller (K-20 MMR Technologies) was used. Data acquisition were computer controlled by custom-written software.[23] Seebeck coefficient measurements were performed using a commercial MMR SB-100 Seebeck Measurement System under vacuum between 308 and 530 K. A needle-like β-$TcCl_2$ crystal was mounted with silver paste in parallel with a constantan reference to monitor the temperature difference across the samples.[24]

Theoretical Methods. First-principles total energy calculations on α-$TcCl_2$ and β-$TcCl_2$ single chains were performed using spin-polarized density functional theory (DFT) as implemented in the

dx.doi.org/10.1021/ja408459k | J. Am. Chem. Soc. 2013, 135, 15955−15962

Vienna *ab initio* simulation package (VASP).[25] The exchange-correlation energy was calculated using the generalized gradient approximation (GGA) with the parametrization of Perdew and Wang (PW91).[26,27] The interaction between valence electrons and ionic cores was described by the projector augmented wave (PAW) method.[28] The Tc(4p,5s,4d) and Cl(3s,3p) electrons were treated explicitly as valence electrons in the Kohn−Sham (KS) equation and the remaining core electrons together with the nuclei were represented by PAW pseudopotentials. The KS equation was solved using the blocked Davidson iterative matrix diagonalization scheme followed by the residual vector minimization method. The plane-wave cutoff energy for the electronic wave functions was set to a value of 350 eV, ensuring the total energy of the system converged to within 1 meV/atom. Periodic supercells containing model linear chains with 12 $[Tc_2^{II}Cl_8]$ units (i.e., $Z = 24$ (Figure 5) were used in the calculations. Chains were oriented along the z axis in a $10 \times 10 \times z$ Å^3 simulation cell. Electronic relaxation was performed with the conjugate gradient method accelerated using the Methfessel-Paxton Fermi-level smearing[29] with a Gaussian width of 0.1 eV. Ionic relaxation was carried out using the quasi-Newton method and the Hellmann−Feynman forces acting on atoms were calculated with a convergence tolerance set to 0.01 eV/Å

Electronic structure calculations on α-$TcCl_2$ and β-$TcCl_2$ extended structures were performed using the self-consistent full-potential linearized augmented plane wave method (LAPW)[30] within density functional theory (DFT)[31] and using the generalized gradient approximation (GGA) of Perdew, Burke and Ernzerhof[32] for the exchange and correlation potentials. The values of the atomic radii were taken to be: 2.0 au for Tc and 2.1 au for Cl atoms, where au is the atomic unit (0.529 Å). Convergence of the self-consistent iterations was performed for 308 k points inside the irreducible Brillouin zone to within 0.0001 Ry with a cutoff of −6.0 Ry between the valence and the core states. The calculations were performed using the WIEN2k program.

RESULTS AND DISCUSSION

Crystallographic Structure. A β-$TcCl_2$ single crystal obtained after the reaction of Tc metal and chlorine was used for the structure determination. Single crystal diffraction experiments revealed additional supercell reflections around the main ones centered at a commensurate distance of $1/2a^* + 1/2b^* + 1/4c^*$. The absence of cross term satellite reflections (reflections coming from the addition and subtraction of modulation vectors) suggested the presence of two twin domains with a single modulation vector rather than a single domain with two individual q-vectors. The commensurate supercell was solved using a (3 + 1)-dimensional crystallographic approach. A tetragonal subcell with $a = b = 8.591(1)$ Å, $c = 3.4251(6)$ Å and a commensurate q-vector at $1/2a^* + 1/2b^* + 1/4c^*$ were used for the structure refinement. The best solution was obtained for the monoclinic superspace group $I2/m(1/21/2\gamma)s0$. The α-$TcCl_2$ polymorph crystallizes in the monoclinic superspace group $P2/m(\alpha\beta0)00$ and a commensurate q-vector at $1/2a^* + 1/2b^*$.[11] Additionally, a pseudomerohedral twin law was used with a corresponding matrix of [0 −1 0 1 0 0 0 0 1] and a refined fraction of 31.7(6)%. The total agreement factor for all the reflections 4977 (1576 main +3402 satellites) was 7.87%, (Table S1, Supporting Information). Since the atomic domain along the fourth dimension was not continuous for the Tc atoms (see contour plot in Figure 2), a special step-like Crenel function was used and centered on the electron density (solid red lines in Figure 2).

The structure of β-$TcCl_2$ consists of infinite chains of face sharing $[Tc_2Cl_8]$ units running along the c-axis (Figure 1). The Tc_2Cl_8 units form tetragonal square prisms with are slightly elongated along the c-axis; in those prisms, the height is ∼8% longer than the edge of the square basis. In the $[Tc_2Cl_8]$ units, the metal−metal separations (i.e., 2.131(2) and 2.142(2) Å) are indicative of a Tc≡Tc triple bonds (*vide infra*). In a chain, two orientations (A and B) of the Tc≡Tc bonds are observed: the Tc≡Tc bonds of two adjacent $[Tc_2Cl_8]$ units being either parallel or perpendicular (Figure 1B). The orientation of the Tc≡Tc bonds changes every two $[Tc_2Cl_8]$ units (i.e., AABBAABB...) and Tc≡Tc bonds with the same orientation have the same length. The distances between Tc≡Tc bonds of parallel (i.e., 3.425(2) Å) and perpendicular $[Tc_2Cl_8]$ units (i.e., 3.744(2) Å) preclude any metal−metal interaction between adjacent units.

The average Tc−Cl distance in the $[Tc_2Cl_8]$ units is 2.398[3] Å. The average bridging <Tc−Cl−Tc> angle between two units with parallel Tc≡Tc bonds (i.e., 91.25[5]°) is smaller than the one between two units with perpendicular Tc≡Tc bonds (i.e., 102.65[5]°). The interatomic distances determined by SCXRD

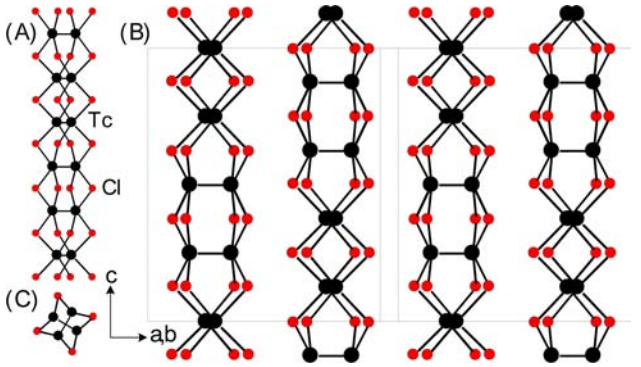

Figure 1. Ball and stick representation of the structure of β-$TcCl_2$. (A) Single β-$TcCl_2$ chain. The orientation of the Tc≡Tc bond changes every two $[Tc_2Cl_8]$ units within a single chain. (B) View along the c-axis of the $2 \times 2 \times 4$ supercell of β-$TcCl_2$ showing the packing of the chains. (C) View down the c-axis of a single β-$TcCl_2$ chain. Tc atoms are in black and chlorine atoms in red.

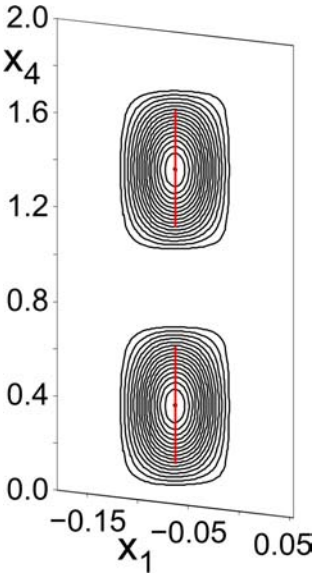

Figure 2. Contour plot of the Tc1 atom along the $x1$(a-axis)-$x4$ (fourth dimension) direction. Each black solid line represents an electron density of 10 e·A^{-3}. Notice that the electron density is not continuous along the forth direction but it has a step-like character. The application of a Crenel function yielded the correct atomic domain shown in solid red lines.

dx.doi.org/10.1021/ja408459k | J. Am. Chem. Soc. 2013, 135, 15955−15962

in β-$TcCl_2$ are in good agreement with the ones found by EXAFS spectroscopy and DFT techniques (Figure 3 and Table

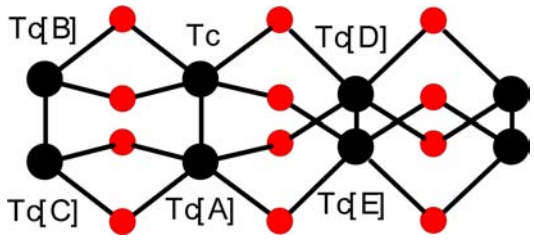

Figure 3. Ball and stick representation of a portion of a β-$TcCl_2$ chain. Tc atoms are in black and chloride atoms are in red.

Table 1. Average Bond Distances (Figure 3) Found by SCXRD, EXAFS,[14] and DFT for β-$TcCl_2$ and Found by SCXRD for α-$TcCl_2$[11] [a]

	SCXRD[b]	EXAFS	DFT	SCXRD[b]
bonds	β-$TcCl_2$	β-$TcCl_2$	β-$TcCl_2$	α-$TcCl_2$
Tc−Tc[A]	2.136(3)	2.13(2)	2.073	2.127(2)
Tc−Cl	2.398(3)	2.42(2)	2.417	2.372(9)
Tc−Tc[B]	3.425(2)	3.45(3)	3.425	3.417(2)
Tc−Tc[C]	4.037(3)	4.01(4)	4.020	4.025(2)
Tc−Tc[D]	3.744(2)	3.79(4)	3.740	[c]

[a]Estimated standard deviations are in parentheses. [b]SCXRD measurements were performed at 100 K for β-$TcCl_2$ and 140 K for α-$TcCl_2$. [c]No perpendicular units are present in α-$TcCl_2$.

1). The structure of β-$TcCl_2$ is closely related to that of α-$TcCl_2$; both dichlorides consist of infinite chains of eclipsed $[Tc_2Cl_8]$ units.[11] In the $[Tc_2Cl_8]$ units, the average Tc−Tc and Tc−Cl distances for β-$TcCl_2$ are slightly larger than the ones found for α-$TcCl_2$ (Table 1). For the two compounds, there are four chains in the reduced subcell that run along the *c*-axis. The volume of the β-$TcCl_2$ reduced subcell (i.e., 252.78(7) Å^3) is slightly larger than the one of α-$TcCl_2$ (i.e., 250.0(2) Å^3). The interchain Cl···Cl distance in β-$TcCl_2$ (i.e., 3.534(2) Å) is larger than the one in α-$TcCl_2$ (3.522(1) Å) and slightly less than the sum of van der Waals radii (3.60 Å).

Physical Properties. The magnetic and transport properties of technetium dichloride were investigated. For the magnetic properties, the compound obtained as the powder (20.1 mg) was placed in a gelatin capsule and the zero field cooled magnetic susceptibility was measured with an applied field of 500 Oe. The representation of the magnetic susceptibility as a function of the temperature (Figure 4A) indicates the compound to be diamagnetic.[33]

The transport properties of technetium dichloride were initially studied by diffuse reflectance spectroscopy. This technique is commonly used to determine optical gaps in semiconductor materials.[34,35] In this method, the optical band gap is determined by fitting the linear portion of the absorption part of the reflectance spectra. For technetium dichloride, the diffuse reflectance spectrum (Figure 4B) was recorded at room temperature on a powder sample. A band gap of 0.12(2) eV was found by fitting the linear portion of the spectrum (Figure 4B; fit in red) indicating that the compound is a narrow gap semiconductor.

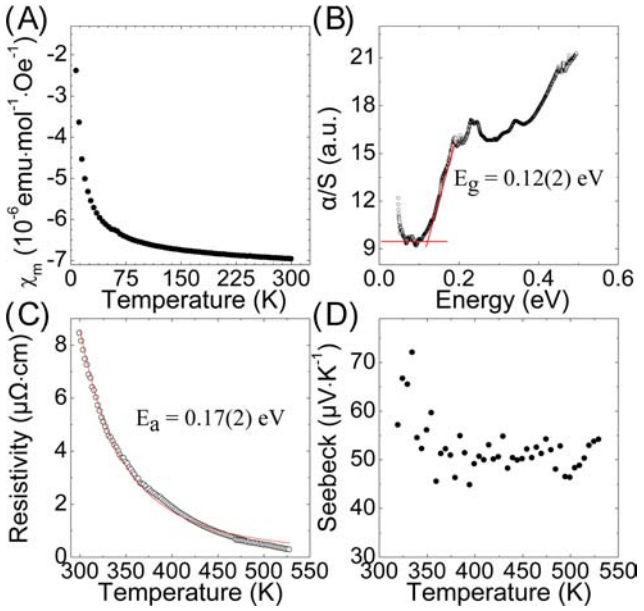

Figure 4. (A) Molar magnetic susceptibility of the $TcCl_2$ powder as a function of temperature showing a diamagnetic response. (B) Diffuse reflectance spectrum of the $TcCl_2$ powder at room temperature. Fit of the absorption edge is in red. (C) Resistivity as a function of temperature of β-$TcCl_2$ single crystal. Red solid line represents the Arrhenius fit with an activation energy of 0.17(2) eV. (D) Seebeck coefficient as a function of temperature of β-$TcCl_2$ showing p-type character.

The semiconducting nature of technetium dichloride was also verified by high temperature electrical resistivity measurements on a β-$TcCl_2$ single crystal. The room-temperature resistivity (Figure 4C) decreases from 8 to 0.3 μΩ·cm at 530 K. The corresponding Arrhenius fit (red solid line in Figure 4C) indicates of a simple mechanism of carrier excitation with an activation energy of 0.17(2) eV. High temperature Seebeck measurement on a β-$TcCl_2$ single crystal (Figure 4D) was positive and in the range of 50−70 μV/K (room temperature to 530 K) suggesting β-$TcCl_2$ is a p-type semiconductor with holes being the dominant type of carriers, Figure 4D.

Computational Studies. To better understand the structure and properties of technetium dichloride, electronic structure calculations were performed on α-$TcCl_2$ and β-$TcCl_2$. Calculations performed on a single β-$TcCl_2$ chain (Figure 5) indicate that bond distances (Tc−Tc = 2.073 Å and Tc−Cl = 2.417 Å), are in good agreement with the experimental data

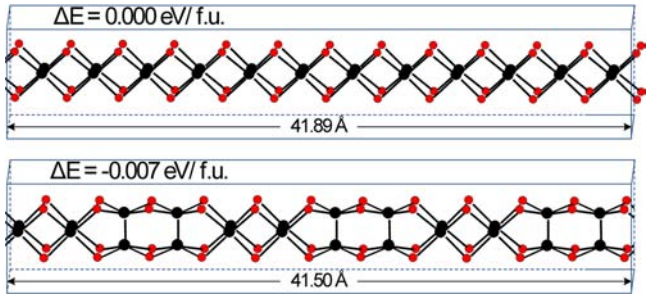

Figure 5. Relaxed structures of α-$TcCl_2$ chains and β-$TcCl_2$ (Z = 24) calculated using spin-polarized density functional theory. The relative total energy difference per formula unit (f.u.), ΔE, is also reported. Tc atoms are in black and Cl atoms are in red.

dx.doi.org/10.1021/ja408459k | J. Am. Chem. Soc. 2013, 135, 15955−15962

(Table 1). Energetic calculations show a difference of 0.007 eV/f.u. between the α-$TcCl_2$ and β-$TcCl_2$ chain, indicating that the β-$TcCl_2$ chain is energetically slightly more favorable than the α-$TcCl_2$ chain.

Further electronic structure calculations at the density functional level were performed in order to study and compare the total energy and band structure of the α-$TcCl_2$ and β-$TcCl_2$ ($2 \times 2 \times 4$ supercell) forms. The possibility of a different orientation and packing of the $TcCl_2$ chains in α-$TcCl_2$ was also examined. Three different models (Figure 6A–C) with different intergrowth forms of α-$TcCl_2$ were examined; calculations indicate Model 1 (Figure 6A) to have the most energetically stable arrangement of α-$TcCl_2$ chains. Models 2 (Figure 6B) and 3 (Figure 6C) are 182 and 200 meV higher in total energy, respectively. The band structure of Model 1 (Figure 6D) suggests a semiconducting behavior with an indirect band gap of around 0.6 eV. Band structures of Model 2 (Figure S3) are similar to Model 1 and indicate either a very narrow semiconducting behavior or a semimetal. In agreement with the experimental results (*vide supra*), the band structure of the supercell of β-$TcCl_2$ (Figure 6E) suggests a semiconductor with an indirect gap of around 0.5 eV.

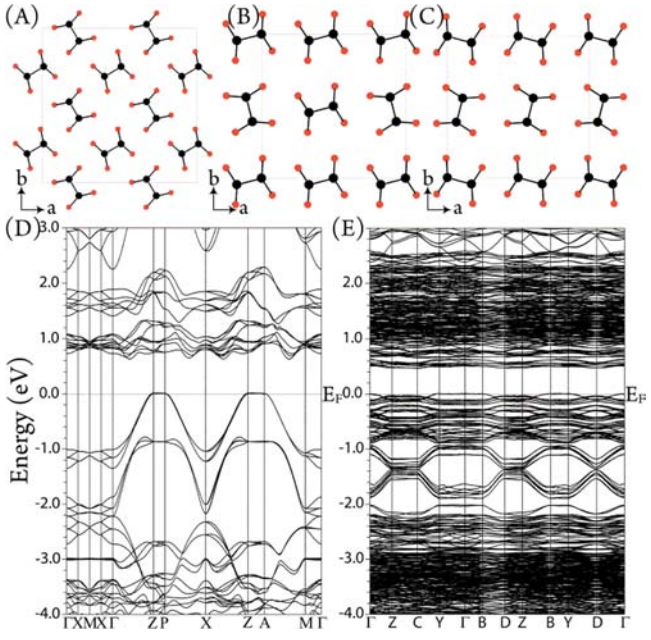

Figure 6. Models used for the calculation of α-$TcCl_2$: Model 1 (A); Model 2 (B); Model 3 (C). Band structure calculation of (D) α-$TcCl_2$ (Model 1) and (E) β-$TcCl_2$.

Review of the Synthesis and Structure of Transition Metal Dichloride. Second and third row transition metal dichlorides can be obtained by many different routes, i.e., reaction between the elements at elevated temperature, thermal decomposition and/or disproportionation of tri- or tetrachloride precursors, reaction between metal-chloride species with gaseous reagents (e.g., Cl_2, HCl) at elevated temperatures, and metallothermic reduction of higher-valent binary chlorides. The various routes are summarized in Table 3.

Technetium dichloride has been obtained by two different routes: (1) reaction between the elements at elevated temperature, and (2) thermal decomposition of $TcCl_4$ under vacuum.

Table 2. Shortest Tc–Tc, Tc–Cl_B, and Tc–Cl_T Distance (Å) in Technetium Binary Chlorides[a]

compound	Tc–Tc	Tc–Cl_B	Tc–Cl_T
α-$TcCl_2$	2.127(2)	2.372(9)	
β-$TcCl_2$	2.136(3)	2.398(3)	
α-$TcCl_3$	2.444(1)	2.373(3)	2.238(2)
β-$TcCl_3$	2.861(3)	2.316(1)	
$TcCl_4$	3.6048(3)	2.3786(3)	2.2355(6)

[a] Cl_B and Cl_T stands for bridging and terminal chloride, respectively.

For the first route, α-$TcCl_2$ and β-$TcCl_2$ were obtained in low yield as single crystals in sealed tubes in different conditions of pressure, deposition temperature and reaction time. Single crystals of β-$TcCl_2$ (yield ~5%), located in the center part of the tube ($T \sim 420$ °C), were obtained congruently with $TcCl_4$ and β-$TcCl_3$ after the reaction of Tc metal and Cl_2 at 450 °C (24 h);[36] these β-$TcCl_2$ crystals were characterized by SCXRD (this work) and EXAFS spectroscopy.[14] In agreement with the X-ray structure, EXAFS spectroscopy shows the presence of parallel and perpendicular Tc_2Cl_8 units in the compound. Concerning α-$TcCl_2$, the black powder obtained after the reaction of Tc metal and Cl_2 at 450 °C was transferred in a second tube, sealed with $AlCl_3$ and reacted at 450 °C; during this experiment, the pressure of Al_2Cl_6 in the tube was estimated at ~1.6 atm. After 4 days of treatments, single crystals of α-$TcCl_2$ were obtained at the cold end of the tube ($T \sim 280$ °C) and used for SCXRD determination.[11] These results emphasize the role of the experimental parameters (reaction time, deposition temperature, pressure, chemical transport agent) on the structure of technetium dichloride; it is anticipated that varying these parameters will lead to other polymorphs of technetium dichloride.

For the second route, $TcCl_4$ decomposes stepwise to α-$TcCl_3$ after 2 h and to $TcCl_2$ after 14 h at 450 °C in a sealed tube under vacuum.[37] Because the formation of α-$TcCl_2$ requires extensive thermal treatment with $AlCl_3$, it is expected that the decomposition product of $TcCl_4$ is β-$TcCl_2$. The thermal behavior of technetium chlorides differ from those of rhenium and are more similar to those of platinum. For rhenium, $ReCl_4$ disproportionates to $ReCl_3$ and $ReCl_5$, the trichloride volatilizes as the Re_3Cl_9 cluster and no decomposition has been reported.[38,39] Similar to technetium, platinum tetra- and trichloride decompose to the dichloride (β-$PtCl_2$).[40] The thermal behavior of technetium tetrabromide[41] has recently been reported.[42] At 450 °C under vacuum in a pyrex ampule, $TcBr_4$ yields the Tc(II) compound $Na\{[Tc_6Br_{12}]_2Br\}$. We note that $PtBr_3$ and $PtBr_4$ are both unstable and decompose to the dibromide.[40]

Among the second and third row transition metals, β-$TcCl_2$ is the 12th dichloride phase to be structurally characterized. Its structure is closely related to that of α-$TcCl_2$, and both compounds consist of infinite chains of eclipsed $[Tc_2Cl_8]$ units.

Polymorphism is common in transition metal dichlorides and two $MoCl_2$, two $PtCl_2$ and four $PdCl_2$ phases have been reported (Table 3). Transition metal dichlorides can be classified into one of four categories, *viz.*, those composed of $[M_2Cl_8]$ units, those composed of square planar MCl_4 units, those containing $[M_6Cl_8]^{4+}$ hexanuclear clusters, and $ZrCl_2$. The various motifs encountered in the dichloride phases are presented in Figure 7.

Dichlorides composed of $[M_2Cl_8]$ units are encountered for technetium (α-$TcCl_2$ (Figure 7A) and β-$TcCl_2$ (Figure 7B))

dx.doi.org/10.1021/ja408459k | J. Am. Chem. Soc. 2013, 135, 15955–15962

Table 3. Second and Third Row Transition Metal MCl_2 Phases (M = Hf, Zr, Mo, W, Tc, Pd and Pt) and Their Method of Synthesis

MCl_2 phase	Experimental conditions
$HfCl_2$[a]	Disproportionation of $HfCl_3$ at 450 °C in a evacuated sealed glass tube.[9]
$ZrCl_2$	Reaction between $ZrCl_4$(g) and ZrCl at 650−750 °C in a sealed tantalum tube under a He atmosphere (≤0.5 atm).[8]
α-$MoCl_2$ (Mo_6Cl_{12})	Disproportionation of $MoCl_3$ at 800 °C in an evacuated, sealed quartz tube.[49] Reduction of $MoCl_5$ with Al in an evacuated, sealed glass tube at 450 °C.[50]
β-$MoCl_2$	Reaction of $Mo_2(O_2CCH_3)_4$ with flowing HCl(g) at 250−350 °C.[51]
WCl_2	Disproportionation of WCl_4 at 450 °C in an evacuated sealed glass tube.[52] Reaction of WCl_6 with Al in an evacuated sealed glass tube at 450 °C.[50]
α-$TcCl_2$	Reaction between the elements in a glass sealed tube at 450 °C followed by treatment (4 days) of the powder 450 °C with $AlCl_3$ in a sealed tube.[11]
β-$TcCl_2$	Reaction between the elements in a glass sealed tube at 450 °C. Decomposition of $TcCl_4$ at 450 °C in an evacuated, sealed glass tube.[37]
α-$PtCl_2$	Treatment of Pt_6Cl_{12} at 500 °C in an evacuated sealed tube.[53] Reaction between the elements in a sealed tube at 550 °C.[53]
β-$PtCl_2$ (Pt_6Cl_{12})	Decomposition of $PtCl_4$ at 350 °C or $PtCl_3$ at 400 °C.[40] Reaction of $H_2PtCl_6{\cdot}6H_2O$ with flowing Cl_2(g) at 475 °C.[53]
γ-$PdCl_2$	Treatment of Pd metal with aqua regia followed by evaporation to dryness and thermal treatment of the resulting solid at 150 °C.[53,54]
α-$PdCl_2$	Treatment of γ-$PdCl_2$ at 400 °C in a glass tube under argon.[54]
δ-$PdCl_2$	Treatment of α-$PdCl_2$ at 500 °C in a glass tube under argon.[54]
β-$PdCl_2$ (Pd_6Cl_{12})	Reaction between Pd and SO_2Cl_2 in an evacuated, sealed glass tube at 400 °C.[55] Reaction between $Pd_3(O_2CCH_3)_6$ with HCl(aq) in acetic acid.[56]

[a]X-ray structure not reported.

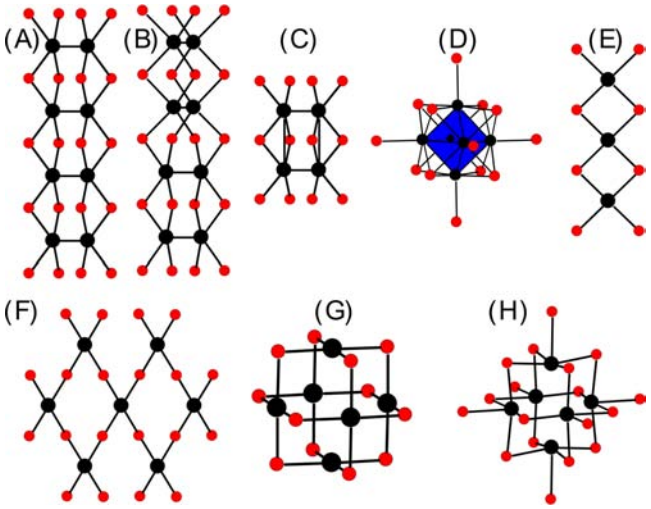

Figure 7. Ball and stick representation of the structural motif in second and third row transition metal dichlorides: (A) α-$TcCl_2$; (B) β-$TcCl_2$; (C) β-$MoCl_2$; (D) α-$MoCl_2$, WCl_2; (E) α-$PtCl_2$, α-$PdCl_2$, δ-$PdCl_2$; (F) γ-$PdCl_2$; (G) β-$PdCl_2$, β-$PtCl_2$; (H) $ZrCl_2$. Metal atoms are in black and Cl atoms are in red.

and molybdenum (β-$MoCl_2$, Figure 7C). For technetium, the structure of α-$TcCl_2$ and β-$TcCl_2$ consists of infinite chains of $[Tc_2Cl_8]$ units (*vide supra*). In the $[Tc_2Cl_8]$ units, the metal−metal separation is characteristic of Tc≡Tc triple bonds.[43] Electronic structure calculations on α-$TcCl_2$ confirm the presence of a triple bond.[11] In these compounds, the Tc≡Tc triple bond exhibits the $\sigma^2\pi^4\delta^2\delta^{*2}$ electronic configuration, which is also in agreement with the diamagnetism of the compound (*vide supra*). The Tc−Tc separation in the $[Tc_2Cl_8]$ unit in β-$TcCl_2$ (i.e, Tc−Tc = 2.136(3) Å) is also similar to the one found in the $Tc_2Cl_8^{3-}$ anion (i.e., Tc−Tc = 2.13(1) Å in $[NH_4]_3Tc_2Cl_8{\cdot}2H_2O$).[44] The influence on the electronic configuration on the metal−metal bonding in complexes with Tc_2^{n+} core (n = 6, 5, 4) has been investigated;[45,46] results indicate that the π component is stronger in the Tc_2^{5+} and Tc_2^{4+} cores than in Tc_2^{6+} core, which is likely the origin of shorter Tc−Tc separation in complexes with Tc_2^{5+} and Tc_2^{6+} cores.

In technetium binary chlorides, the electronic configuration of the Tc atoms has an effect on the metal−metal separation in the coordination polyhedra and the Tc−Tc separation (Δ_{TcTc}) follows the order: $\Delta_{TcTc}(\beta\text{-}TcCl_2) \approx \Delta_{TcTc}(\alpha\text{-}TcCl_2) < \Delta_{TcTc}(\alpha\text{-}TcCl_3) < \Delta_{TcTc}(\beta\text{-}TcCl_3) < \Delta_{TcTc}(TcCl_4)$ (Table 2). For the Tc−Cl_B (Bridging) and Tc−Cl_T (Terminal) separation, the electronic configuration has a minimal effect and no trends are observed.

For β-$MoCl_2$, a single crystal X-ray structure is still elusive, but EXAFS measurements revealed the presence of the $[Mo_4Cl_{12}]$ unit.[14] The latter consists of two face-sharing $[Mo_2Cl_8]$ units, and the Mo(μ-Cl)$_2$Mo separations are consistent with Mo−Mo single bonds between the $[Mo_2Cl_8]$ units. The metal−metal separation in $[Mo_2Cl_8]$ (Table 4) is indicative of a Mo≡Mo triple bond.[43] The presence of single and triple bonds in β-$MoCl_2$ is in agreement with the low magnetic susceptibility of the compound.[47,48]

Table 4. Shortest Metal−Metal Separation (M−M in Å) in Second and Third Row Transition Metal Dichlorides

phase	M−M (Å)	phase	M−M (Å)
$ZrCl_2$	3.3819(3)[8]	α-$PtCl_2$	3.073(4)[61]
α- $MoCl_2$	2.61(1)[49]	β-$PtCl_2$	3.319(2)[62]
β-$MoCl_2$	2.21(2)[14]	α-$PdCl_2$	3.339(2)[54]
WCl_2	Not reported[49]	β-$PdCl_2$	3.283(1)[63]
α-$TcCl_2$	2.129(1)[11]	δ-$PdCl_2$	3.288(1)[54]
β-$TcCl_2$	2.131(2)[a]	γ-$PdCl_2$	3.742(2)[54]

[a]This work.

Dichlorides composed of the $[M_6Cl_8]^{4+}$ clusters are found for tungsten and molybdenum, Figure 7D. In these compounds, the octahedral $[M_6]^{12+}$ core is bonded to eight face-capping Cl ligands ($[M_6Cl_8]^{4+}$) and six terminal chlorine ligands.[10,49] The crystallographic and electronic structure of the $[M_6Cl_8]^{4+}$ clusters have been extensively studied, and the results indicate the presence of metal−metal single bonds.[57−60] The $[M_6]^{12+}$ core has 24 electrons shared between 12 single bonds, which is in agreement with the diamagnetism of the compounds.[60]

Dichlorides composed of square planar MCl_4 units are encountered for platinum and palladium. Their structures can

dx.doi.org/10.1021/ja408459k | J. Am. Chem. Soc. 2013, 135, 15955−15962

either consist of infinite chains of edge-sharing MCl_4 units (α-$PtCl_2$,[61] α-$PdCl_2$,[12,54] δ-$PdCl_2$,[54] Figure 7E), infinite layers of corner-sharing MCl_4 (γ-$PdCl_2$, Figure 7F)[54], or M_6Cl_{12} cubic clusters composed of four edge-sharing MCl_4 units (β-$PtCl_2$[62,64] and β-$PdCl_2$,[63,65] Figure 7G). In those phases, the shortest metal−metal separation (Table 3) ranges from 3.073(3) Å in α-$PtCl_2$[61] to 3.742(2) Å in γ-$PdCl_2$;[54] these distances are larger than those expected for Pt−Pt and Pd−Pd single bonds.[43] Analysis of the electronic structure of β-$PtCl_2$ suggests that minimal metal−metal interaction occurs in the Pt_6Cl_{12} cubic cluster.[66] In the platinum and palladium dichlorides, the metals have a d^8 electron configuration and those compounds are diamagnetic.[67]

Finally, $ZrCl_2$ consists of infinite layers of edge sharing deformed $ZrCl_6$ octahedra (Figure 7H).[8] The metal−metal separation, 3.3819(3) Å, is close to the one expected for single Zr−Zr bond.[43] The low magnetic susceptibility of $ZrCl_2$ is consistent with the presence of discrete metal−metal interactions in the compound.[68]

Concerning transport properties, β-$TcCl_2$ is a semiconductor with a band gap of 0.12(2) eV. To the best of our knowledge, it is the lowest band gap reported for a transition metal dichloride. Zirconium dichloride is also a semiconductor and an activation energy of around 0.3 eV has been estimated from resistivity measurements.[8] The semiconducting nature of β-$TcCl_2$ contrasts with α-$MoCl_2$ which is an insulator.[69] Concerning $PtCl_2$ and $PdCl_2$, no resistivity measurements have been performed.

CONCLUNDING REMARKS

A second polymorph of technetium dichloride, β-$TcCl_2$, has been synthesized from the reaction of Tc metal and chlorine in a sealed tube at 450 °C. The crystallographic structure and physical properties β-$TcCl_2$ have been investigated. The structure of β-$TcCl_2$ is similar to that of α-$TcCl_2$ with an additional long-range ordering of Tc≡Tc vectors and consists of infinite chains of face sharing $[Tc_2Cl_8]$ units; within a chain, the Tc≡Tc vectors of two adjacent $[Tc_2Cl_8]$ units are either perpendicular or parallel. In agreement with theoretical calculations, resistivity measurements indicate β-$TcCl_2$ to be a semiconductor while a magnetic susceptibility measurement shows the compound to be diamagnetic. A Seebeck measurement suggests β-$TcCl_2$ is a p-type semiconductor. The discovery of β-$TcCl_2$ brings to 12 the number of transition metal dichloride phases structurally characterized. Currently, nine technetium binary halide phases are known (TcF_6, TcF_5, $TcBr_4$, $TcBr_3$, $TcCl_4$, α/β-$TcCl_3$, α/β-$TcCl_2$) and it is anticipated that this number will increase. Because technetium dichloride can be obtained from the thermal decomposition of $TcCl_4$ and/or from the reaction of the elements in a sealed tube, it is still an open question whether $TcBr_2$ is accessible by these methods and whether its structure will be similar to that of $TcCl_2$ or a Tc_6Br_{12} cluster. In this context, the thermal decomposition of $TcBr_4$ in Pyrex has been studied and provides low yields of $Na\{[Tc_6Br_{12}]_2Br\}$; the latter contains the Tc_6Br_{12} trigonal prismatic cluster.[42] The reaction between Tc and Br_2 (Tc/Br, 1:2) has not yet been performed and is under investigation. Binary technetium iodides are still unknown and their preparation is being investigated in our laboratories. Finally, we note that rhenium dichloride is unknown. This is surprising in view of the existence of numerous metal−metal bonded rhenium(II) complexes.[70] We anticipate that $ReCl_2$ might be obtained from the metallothermic reduction of $ReCl_3$.

ASSOCIATED CONTENT

Supporting Information

Additional synthetic and characterization details; crystallographic tables; band structure calculations of Model 2 and Model 3. This material is available free of charge via the Internet at http://pubs.acs.org.

AUTHOR INFORMATION

Corresponding Author

asattelberger@anl.gov.

Notes

The authors declare no competing financial interest.

ACKNOWLEDGMENTS

Funding for this research was provided by an NEUP grant from the U.S. Department of Energy, Office of Nuclear Energy, through INL/BEA, LLC, 00129169, agreement No. DE-AC07-05ID14517. Sandia National Laboratories is a multiprogram laboratory managed and operated by Sandia Corporation, a wholly owned subsidiary of Lockheed Martin Corporation, for the U.S. Department of Energy's National Nuclear Security Administration under contract DE-AC04-94AL85000. The authors thank Trevor Low and Julie Bertoia for outstanding health physics support. This work was also supported by the U.S. Department of Energy, Office of Basic Energy Sciences under contract no. DE-AC02-06CH11357.

REFERENCES

(1) Canterford, J. H.; Colton, R. *Halides of the Second and Third Row Transition Metals*; John Wiley and Sons: New York, 1968.
(2) Cotton, F. A.; Wilkinson, G.; Murillo, C. A.; Bochmann, M. *Advanced Inorganic Chemistry*, 6th ed.; John Wiley and Sons: New York, 1999.
(3) Ghosh, R. N.; Baker, G. L.; Ruud, C.; Nocera, D. G. *Appl. Phys. Lett.* **1999**, *75*, 2885.
(4) Gray, T. G. *Coord. Chem. Rev.* **2003**, *243*, 213.
(5) Kamiguchi, S.; Nagashima, S.; Komori, K.-i.; Kodomari, M.; Chihara, T. *J. Cluster Sci.* **2007**, *18*, 414.
(6) Ströbele, M.; Jüstel, T.; Bettentrup, H.; Meyer, H. J. *Z. Anorg. Allg. Chem.* **2009**, *635*, 822.
(7) Blomstrand, W. *J. Prakt. Chem.* **1859**, *77*, 88.
(8) Cisar, A.; Corbett, J. D.; Daake, R. L. *Inorg. Chem.* **1979**, *18*, 836.
(9) Larsen, E. M.; Leddy, J. J. *J. Am. Chem. Soc.* **1956**, *78*, 5983.
(10) Biltz, W.; Fendius, C. *Z. Anorg. Allg. Chem.* **1928**, *172*, 385.
(11) Poineau, F.; Malliakas, C. D.; Weck, P. F.; Scott, B. L.; Johnstone, E. V.; Forster, P. M.; Kim, E.; Kanatzidis, M. G.; Czerwinski, K. R.; Sattelberger, A. P. *J. Am. Chem. Soc.* **2011**, *133*, 8814.
(12) Wells, A. F. *Z. Kristallogr.* **1938**, *100*, 189.
(13) Brodersen, K. *Angew. Chem.* **1964**, *76*, 690.
(14) Poineau, F.; Johnstone, E. V.; Weck, P. F.; Kim, E.; Conradson, S. D.; Sattelberger, A. P.; Czerwinski, K. R. *Inorg. Chem.* **2012**, *51*, 4965.
(15) *X-AREA*; STOE & Cie GmbH, IPDS Software: Darmstadt, 2006.
(16) Petricek, V.; Dusek, M.; Palatinus, L. In *The Crystallographic Computing System*; Institute of Physics: Praha, Czech Republic, 2006.
(17) Sheldrick, G. M. *SHELXTL*, Version 6.14; Bruker Analytical X-Ray Instruments, Inc.: Madison, WI, 2003.
(18) Petricek, V.; Vanderlee, A.; Evain, M. *Acta Crystallogr., Sect. A* **1995**, *51*, 529.
(19) Boucher, F.; Evain, M.; Petricek, V. *Acta Crystallogr., Sect. B* **1996**, *52*, 100.
(20) Kortüm, G. *Reflectance Spectroscopy: Principles, Methods, Applications*; Springer-Verlag: New York, 1969.

(21) Tandon, S. P.; Gupta, J. P. *Phys. Status Solidi B* **1970**, *38*, 363.
(22) Wendlandt, W. W.; Hecht, H. G. *Reflectance Spectroscopy*; Interscience Publishers: New York, 1966.
(23) Malliakas, C. D. Specialized scripts written in LabView were utillized to collect an $I-V$ curve of 11 points from +10 to −10 μA on each temperature point from 300 to 530 K with a step of 2 K.
(24) The size of the β-$TcCl_2$ needle crystal was much smaller and thinner than the constantan reference; therefore, the thermal gradient along the two samples is quite different and the calculated Seebeck coefficient may deviate from the true value.
(25) Kresse, G.; Furthmuller, J. *Phys. Rev. B* **1996**, *54*, 11169.
(26) Perdew, J. P.; Chevary, J. A.; Vosko, S. H.; Jackson, K. A.; Pederson, M. R.; Singh, D. J.; Fiolhais, C. *Phys. Rev. B* **1992**, *46*, 6671.
(27) Perdew, J. P.; Wang, Y. *Phys. Rev. B* **1992**, *45*, 13244.
(28) Blöchl, P. E. *Phys. Rev. B* **1994**, *50*, 17953.
(29) Methfessel, M.; Paxton, A. T. *Phys. Rev. B* **1989**, *40*, 3616.
(30) Singh, D. *Planewaves, Pseudopotentials, and the LAPW Method*; Kluwer Academic: Boston, MA, 1994.
(31) Kohn, W.; Sham, L. J. *Phys. Rev.* **1965**, *140*, 1133.
(32) Perdew, J. P.; Burke, K.; Ernzerhof, M. *Phys. Rev. Lett.* **1996**, *77*, 3865.
(33) The measured magnetic susceptibility was corrected for the paramagnetic contribution of unreacted Tc present in the sample. The ratio of $Tc/TcCl_2$ was refined by powder X-ray diffraction analysis to 13/87.
(34) Korlann, S. D.; Riley, A. E.; Kirsch, B. L.; Mun, B. S.; Tolbert, S. H. *J. Am. Chem. Soc.* **2005**, *127*, 12516.
(35) Riley, A. E.; Tolbert, S. H. *J. Am. Chem. Soc.* **2003**, *125*, 4551.
(36) Poineau, F.; Johnstone, E. V.; Weck, P. F.; Forster, P. M.; Kim, E.; Czerwinski, K. R.; Sattelberger, A. P. *Inorg. Chem.* **2012**, *51*, 4915.
(37) Johnstone, E. V.; Poineau, F.; Forster, P. M.; Ma, L.; Hartmann, T.; Cornelius, A.; Antonio, D.; Sattelberger, A. P.; Czerwinski, K. R. *Inorg. Chem.* **2012**, *51*, 8462.
(38) Christodoulakis, A.; Maronitis, C.; Boghosian, S. *Phys. Chem. Chem. Phys.* **2001**, *3*, 5208.
(39) Frais, P. W.; Guest, A.; Lock, C. J. L. *Can. J. Chem.* **1969**, *47*, 1069.
(40) Degner, M.; Holle, B.; Kamm, J.; Pilbrow, M.; Thiele, G.; Wagner, D.; Weigl, W.; Woditsch, P. *Transition Met. Chem.* **1975**, *1*, 41.
(41) Poineau, F.; Rodriguez, E. E.; Forster, P. M.; Sattelberger, A. P.; Cheetham, A. K.; Czerwinski, K. R. *J. Am. Chem. Soc.* **2008**, *131*, 910.
(42) Johnstone, E. V.; Grant, D. J.; Poineau, F.; Fox, L.; Forster, P. M.; Ma, L.; Gagliardi, L.; Czerwinski, K. R.; Sattelberger, A. P. *Inorg. Chem.* **2013**, *52*, 5660.
(43) Pyykkö, P.; Atsumi, M. *Chem.—Eur. J.* **2009**, *15*, 12770.
(44) Bratton, W. K.; Cotton, F. A. *Inorg. Chem.* **1970**, *9*, 789.
(45) Poineau, F.; Forster, P. M.; Todorova, T. K.; Gagliardi, L.; Sattelberger, A. P.; Czerwinski, K. R. *Inorg. Chem.* **2010**, *49*, 6646.
(46) Poineau, F.; Forster, P. M.; Todorova, T. K.; Gagliardi, L.; Sattelberger, A. P.; Czerwinski, K. R. *Dalton Trans.* **2012**, *41*, 2869.
(47) Allison, G. B.; Anderson, I. R.; Sheldon, J. C. *Aust. J. Chem.* **1969**, *22*, 1091.
(48) Ryan, T. R.; McCarley, R. E. *Inorg. Chem.* **1982**, *21*, 2072.
(49) Schäfer, H.; Schnering, H. G. V.; Tillack, J.; Kuhnen, F.; Wöhrle, H.; Baumann, H. *Z. Anorg. Allg. Chem.* **1967**, *353*, 281.
(50) Dorman, W. C.; McCarley, R. E. *Inorg. Chem.* **1974**, *13*, 491.
(51) Glicksman, H. D.; Hamer, A. D.; Smith, T. J.; Walton, R. A. *Inorg. Chem.* **1976**, *15*, 2205.
(52) McCarley, R. E.; Brown, T. M. *Inorg. Chem.* **1964**, *3*, 1232.
(53) Chusova, T. P.; Semenova, Z. I. *Thermochim. Acta* **2009**, *482*, 62.
(54) Evers, J.; Beck, W.; Göbel, M.; Jakob, S.; Mayer, P.; Oehlinger, G.; Rotter, M.; Klapötke, T. M. *Angew. Chem., Int. Ed.* **2010**, *49*, 5677.
(55) Dillamore, I. M.; Edwards, D. A. *J. Inorg. Nucl. Chem* **1969**, *31*, 2427.
(56) Yatsimirski, A.; Ugo, R. *Inorg. Chem.* **1983**, *22*, 1395.
(57) Simon, A. *Angew. Chem., Int. Ed. Engl.* **1988**, *27*, 159.
(58) Prokopuk, N.; Shriver, D. F. In *Advances in Inorganic Chemistry*; Sykes, A. G., Ed.; Academic Press: New York, 1998; Vol. *46*, p 1.
(59) Cotton, F. A.; Haas, T. E. *Inorg. Chem.* **1964**, *3*, 10.
(60) Kepert, D. L.; Vrieze, K. *Halogen Chem.* **1967**, *3*, 1.
(61) Krebs, B.; Brendel, C.; Schäfer, H. *Z. Anorg. Allg. Chem.* **1988**, *561*, 119.
(62) von Schnering, H. G.; Chang, J.-H.; Peters, K.; Peters, E.-M.; Wagner, F. R.; Grin, Y.; Thiele, G. *Z. Anorg. Allg. Chem.* **2003**, *629*, 516.
(63) Dell'Amico, D. B.; Calderazzo, F.; Marchetti, F.; Ramello, S. *Angew. Chem., Int. Ed. Engl.* **1996**, *35*, 1331.
(64) Brodersen, K.; Thiele, G.; Schnering, H. G. *Z. Anorg. Allg. Chem.* **1965**, *337*, 120.
(65) Schäfer, H.; Wiese, U.; Rinke, K.; Brendel, K. *Angew. Chem., Int. Ed. Engl.* **1967**, *6*, 253.
(66) Kettle, S. F. A. *Nature* **1966**, *209*, 1021.
(67) van Bronswyk, W.; Nyholm, R. *J. Chem. Soc. A* **1968**, 2084.
(68) Lewis, J.; Machin, D. J.; Newnham, I. E.; Nyholm, R. S. *J. Chem. Soc.* **1962**, 2036.
(69) Perrin, C.; Sergent, M. *J. Less-Common Met.* **1986**, *123*, 117.
(70) Cotton, F. A.; Murillo, C. A.; Walton, R. A. In *Multiple Bonds between Metal Atoms*; 3rd ed.; Springer: New York, 2005.